Silicon oxide multilayer coatings doped with carbon nanotubes and graphene nanoplatelets for corrosion protection of AZ31B magnesium alloy

J.P. Fernández-Hernán, A.J. López[*], B. Torres, J. Rams.*

Área de ciencia e ingeniería de materiales, ESCET, Universidad Rey Juan Carlos, C/ Tulipán, s/n, Móstoles 28933, Madrid, España.

ABSTRACT

Magnesium (Mg) AZ31B alloy substrates were coated by the dip-coating method to obtain four different coating configurations. Three different sol-gels were synthesized to create different monolayer and multilayer coating configurations from two silicon alkoxides, tetraethyl orthosilicate (TEOS) and methyl-triethoxysilane (MTES). Two of these sol-gel solutions were doped with nanocharges. The final concentration of nanocharges in the coatings was 0.045 wt% and 0.046 wt% for multiwall carbon nanotubes (MWCNTs) and functionalized graphene nanoplatelets (COOH-GNPs), respectively. The anti-corrosion behaviour of these coatings was assessed by electrochemical and hydrogen evolution tests in 3.5 wt% NaCl solution. All of the coating configurations significantly improved the behaviour against corrosion compared with the bare substrate, especially the SG+SG/GNP (sol-gel + sol-gel doped with 0.046 wt% COOH-GNPs) multilayer coating system. The sol-gel synthesis combined with the dip-coating method was demonstrated to be an effective way to generate compact and homogeneous coatings for corrosion protection.

Keywords: Magnesium; Corrosion; Coating; Sol-Gel; Carbon nanotubes; Graphene nanoplatelets.

[*] *Corresponding author: Dr. Antonio Julio López Galisteo;*
Tel.: +34 4887131; e-mail: antoniojulio.lopez@urjc.es

1. Introduction

In recent years, the transport sector has been facing some challenges that must be solved in the short/mid-term. One of these challenges is to decrease the consumption of fossil fuels and to drastically reduce toxic emissions to the atmosphere. Because of these challenges, new technologies like electric vehicles have been developed, but these new kinds of vehicles present new handicaps, for example, the autonomy of electric batteries. One solution that could help to overcome these challenges is a weight reduction of the vehicles. At this point, magnesium and magnesium alloys become interesting. Among the structural metals, magnesium has the lowest density value (ρ_{Mg} = 1,74 g/cm^3) and a strength/weight ratio better than aluminium and steel [1]. Therefore, magnesium could be a good choice for the manufacture of lighter structural parts for vehicles.

In spite of its outstanding properties, the fact that magnesium and its alloys are not widespread in the transport sector is because of their main drawback which is that magnesium is a very reactive metal and prone to suffer from corrosion processes. Moreover, the corrosion products are not resistant enough to create an effective passivation layer. [2][3][4][5]

One strategy that is usually followed to improve corrosion resistance is to generate coatings on the surface of the metallic substrates to isolate them from the aggressive media, in order to avoid or retard the corrosion processes. Coatings generated by the sol-gel process have been deeply studied, [6][7][8][9]. Sol-gel synthesis is an easy, low-cost and eco-friendly method to synthesize hybrid organic-inorganic materials that can be used to generate micrometric, homogeneous and crack-free coatings. During the sol-gel synthesis process, the hydrolysis and polycondensation of the colloidal particles of the starting solution (sol) lead to the generation of a three-dimensional interconnected network (gel) which, after a drying and aging process, becomes a solid monolith of material [10][11].

The use of hybrid coatings solves some of the main drawbacks of pure inorganic or pure organic coatings. Inorganic coatings are brittle and tend to crack when a thickness bigger than 1 µm is achieved. The use of hybrid coatings makes it possible to obtain thicker coatings without cracking [8][12][13]. Drying and a thermal sintering treatment are necessary to obtain coatings with good properties. Relatively high temperatures are required (400 ^{o}C – 800 ^{o}C) in the case of oxide inorganic coatings, or temperatures up to 150 ^{o}C in the case of hybrid inorganic-organic coatings [11][14][15]. For oxide layers, the temperature is a major drawback when the coated substrate is a magnesium alloy whose melting point is found around 650 ^{o}C.

Based on different studies [16][17][18][19][20], the addition of nanocharges, such as carbon nanotubes and graphene nanoplatelets, during the sol-gel synthesis could make it possible to obtain coatings with improved mechanical properties and enhanced protection against corrosion.

There are several deposition methods used to coat a substrate. The dip-coating technique is useful to obtain coatings with a specific thickness by controlling the extraction speed of the substrate which is meant to be coated from the volume of the coating material [21][22].

The objective of this research is to assess the anticorrosion behaviour of different coating systems generated by sol-gels from two silicon alkoxides coated on AZ31B magnesium alloy substrates.

2. Experimental

2.1 Substrate material

AZ31B magnesium alloy samples were obtained from a plate of 300x300x5 mm provided by Magnesium Elektron. The composition of this alloy in weight percent is: 2.9 Al, 0.75 Zn, 0.29 Mn, 0.01 Si, <0.005 Ca, 0.004 Fe, 0.0013 Ni, and <0.0005 Cu; the balance is Mg. The final substrate samples were cut in an orthogonal volume of 20x20x3 mm^3. Before coating, all

substrates were ground to 1200 SiC grit papers, degreased in an ultrasonic isopropanol bath for 10 minutes, and air-dried.

2.2 Nanocharges

Two different types of nanocharges were used in this research as nano-reinforcement for the different coating systems. NC7000 multiwall carbon nanotubes provided by Nanocyl (Fig.1a). The MWCNTs appear entangled when they are in the powder state from the manufacturer. In the inset of Fig.1a MWCNT detail can be seen. These nanocharges present an average diameter of 9.5 nm and an average length of 1.5 μm. Grade 4 COOH-functionalized graphene nanoplatelets provided by Cheap Tubes Inc. in powder state from the manufacturer (Fig.1b). These nanocharges present an average size of 2 μm and a thickness value lower than 4 nm.

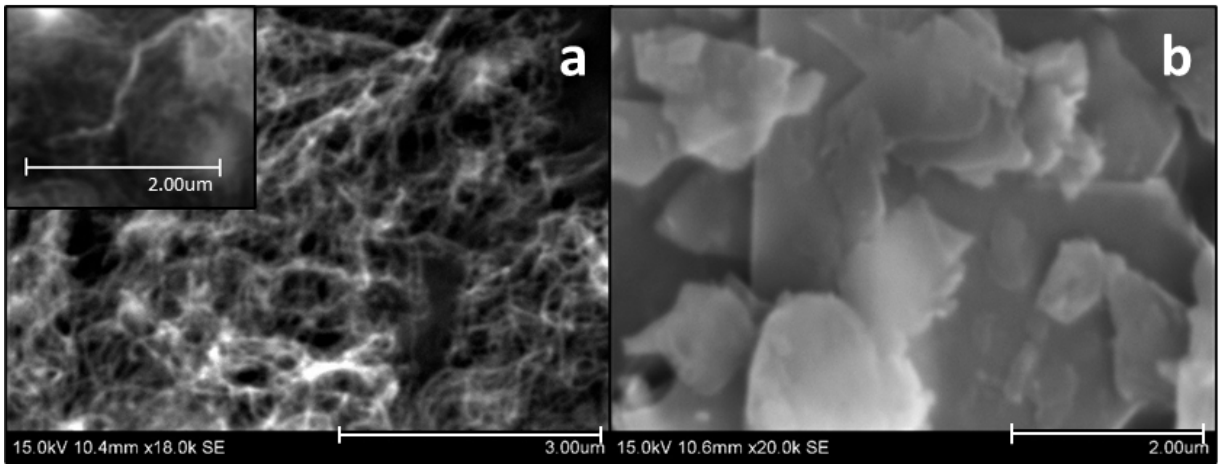

Fig. 1. SEM micrographs of the MWCNTs (a) and the COOH-GNPs (b) used as nano-reinforcement.

2.3 Coating generation and deposition

Four different hybrid silica mono- and multilayer coating systems were obtained by the combination of three different initial sols. The compositions of the three initial sols (A, B, and C) are shown in Table 1. These sols were prepared from two silicon alkoxides: tetraethyl orthosilicate (TEOS; $Si(C_2H_5O)_4$) and methyl-triethoxysilane (MTES; CH_3-$Si(C_2H_5O)_3$). The initial mixtures of these two precursors were diluted in isopropanol and 0.1M HCl acidulated

H_2O. Furthermore, two of these sols were doped with nanocharges: 0.005 wt% of MWCNTs were added to Sol B and 0.005 wt% of COOH-GNPs were added to Sol C.

Table 1. Composition of the three different sol-gels used to generate the coatings.

Sol-gel	Composition (molar ratio = 1:5:10)	Nanocharges (wt%)
Sol A	40% TEOS/60% MTES : Isopropanol : 0.1M HCl-H_2O	-
Sol B	40% TEOS/60% MTES : Isopropanol : 0.1M HCl-H_2O	0.005 MWCNTs
Sol C	40% TEOS/60% MTES : Isopropanol : 0.1M HCl-H_2O	0.005 COOH-GNPs

The molar ratio of these compounds in the starting sols was TEOS + MTES/Isopropanol/water: 1/5/10. To obtain the initial sols, TEOS and MTES were mixed in molar fraction of 40%/60% for 30 minutes with magnetic stirring; this rate was determined after different tests. In different beakers, nanocharges were added to isopropanol and ultrasonically dispersed for 10 minutes. To obtain the sol named B, 0.005 wt% MWCNTs were added to isopropanol. To obtain the sol named C, 0.005 wt% COOH-GNPs were added to isopropanol. No nanocharges were added to isopropanol to obtain the sol named A. The final concentrations of nanocharges measured in the coatings were 0.045 wt% of non-functionalized MWCNTs and 0.046 wt% of COOH-GNPs.

TEOS/MTES and isopropanol (with or without nanocharges) were mixed by magnetic stirring for 10 minutes. Then, acidulated distilled water was added to each of the three different sols. and the final mixture was magnetically stirred at 300 rpm for 2 hours at room temperature. Finally, all of the sols were left standing for 30 minutes without stirring at room temperature in order to allow the hydrolysis and polycondensation reactions to be completed.

Once the sols were synthesized, AZ31B substrates were homogeneously coated by the dip-coating method. The extraction direction from the sol-gel for all the coating configurations was perpendicular to the grounding lines of the substrates. Then a low-temperature and long-lasting

thermal treatment consisting of 24 h at 100 ºC followed by 24 h at 200 ºC was applied in order to avoid problems from the different coefficients of thermal expansion of AZ31B substrate and silicon oxide coatings that may cause cracks in the coating and taking into account the influence of temperature on corrosion resistance [14][23]. Four different coating configurations were evaluated (Fig.2):

(i) Monolayer coating without nanocharges (SG) from the sol A ; (ii) multilayer coating without nanocharges composed of two layers (SG+SG) from the sol A; (iii) multilayer coating composed of a first layer from the sol A, without nanocharge, and a second layer from sol B with a final concentration in the coating of 0.045 wt% MWCNTs (SG+SG/CNT); (iv) multilayer coating composed of a first layer from the sol A, without nanocharge, and a second layer from sol C with a final concentration in the coating of 0.046 wt% COOH-GNPs (SG+SG/GNP). The coating process for all the different coating configurations was as follows:

For the SG monolayer coating, the substrates were immersed in sol A for 1 minute and extracted with a withdrawal speed of 35 cm/min. Then the thermal treatment previously described was applied to the coated samples. Finally, the samples were cooled inside the oven.

In the case of multilayer systems, for all of the samples, the first layer was applied by the immersion of the metallic substrates in sol A for 1 minute and then extraction with a withdrawal speed of 35 cm/min. This first layer was dried at 100 ºC for 1 hour. Then, the second layer was applied by immersion of the samples in the respective sols for each coating configuration (sol A for the SG+SG system, sol B for the SG+SG/CNT system, and sol C for the SG+SG/GNP system), and then the extraction was done at 35 cm/min. All of the multilayer systems were dried at room temperature for 1 minute, rinsed with distilled water to remove the excess of material, dried at 100 ºC for 24 hours, and then sintered at 200 ºC for 24 hours and cooled inside the oven.

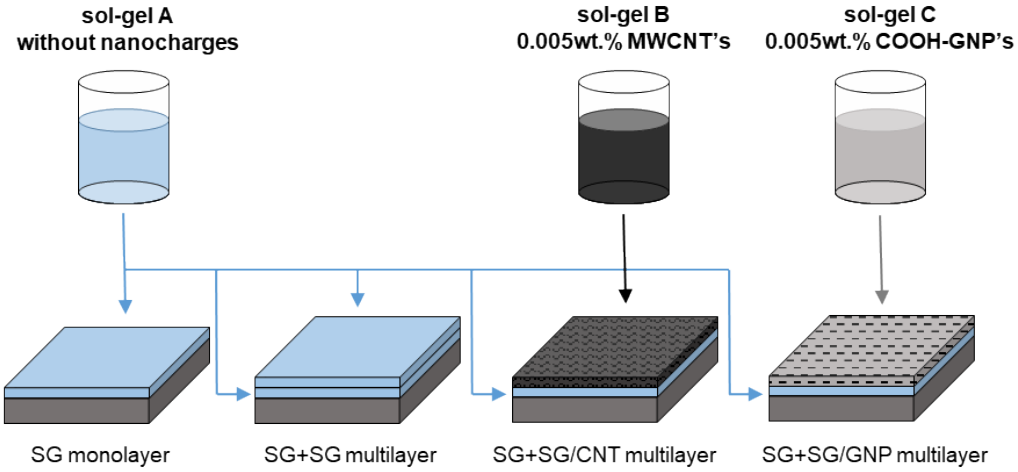

Fig.2. Four different coating configurations: SG monolayer, SG+SG multilayer, SG+SG/CNT multilayer, SG+SG/GNP multilayer.

2.4 Coating characterization

A scanning electron microscope (Hitachi, S-3400N) was used to determine the presence of cracks and to measure the thickness of the coatings before corrosion tests, as well as to assess the dispersion state of the nanocharges in the coatings. Coated samples were mounted in resin and then cut, ground, and polished to prepare them to be observed in a cross-sectional view. The thickness of the different coating systems was measured in the central zone of the samples. Transmission electron microscopy (Philips Tecnai 20T) was used to assess the dispersion state of the nanocharges embedded in the sol-gel coatings. The roughness tester (Mitutoyo SJ-210) was used to assess the surface roughness of the different coating configurations and the roughness of the uncoated substrate in order to study how the deposition of the different coating systems affects this parameter.

2.5 Corrosion tests

Electrochemical linear polarization resistance tests were carried out to determine the instantaneous corrosion rate [24] with a Metrohm Autolab PGSTAT302N potentiostat using a three-electrode cell configuration. The sample was the working electrode, an Ag/AgCl electrode was the reference electrode, and a graphite rod was the counter electrode (Fig.3a).

Samples were immersed in a 3.5 wt% NaCl solution at room temperature. After a stabilization time, polarization resistance (*Rp*) was measured at 1 hour and then every 24 hours until the total time of immersion of 168 hours with an applied potential of ±10 mV around the corrosion potential (E_{corr}) and a scanning rate of 1 mV/s.

Anodic-cathodic polarization analysis, also known as Tafel test, was carried out at room temperature with the same cell configuration as in the polarization resistance test. Two different immersion times were evaluated. A set of samples was immersed in a 3.5 wt% NaCl solution for 1 hour, and the other set of samples was immersed in 3.5 wt% NaCl for 24 hours. In both cases, after a stabilization time of the corrosion potential (E_{corr}), the procedure was carried out with a scanning range of 1000 mV (-400 mV / +600 mV) around (E_{corr}).

The hydrogen evolution test is an easy and accurate method to assess the corrosion rate of magnesium and its alloys [25]. These tests were carried out at room temperature to measure the hydrogen liberated during the corrosion processes in 3.5 wt% NaCl solution. This test estimates the corrosion rate of magnesium samples, based on the corrosion reaction of magnesium and the hydrogen evolution produced as a sub-product of the corrosion reaction, as described by Song et al. [5][25] In the present work, the experiments lasted a total time of 168 hours. The samples were mounted into a cell with a 0.75 cm^2 surface exposed to the chloride solution. A funnel was placed over the sample and connected to a burette that was used to collect and measure the hydrogen liberated from the corroded area of the sample. (Fig.3b)

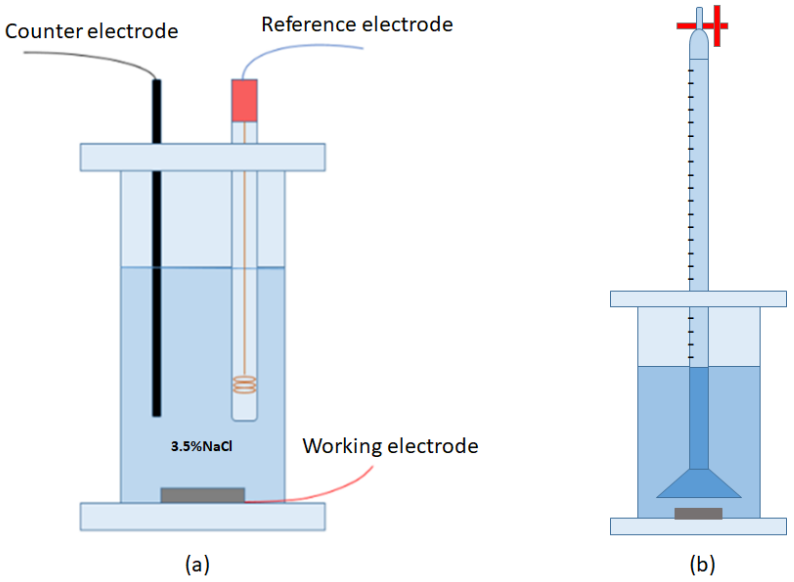

Fig.3. Experimental set-up. (a) Three-electrode cell configuration for electrochemical polarization resistance tests. (b) Sample mounted for hydrogen evolution test.

The weight of the samples was measured (Sartorius BP221S) before and after the hydrogen evolution test to perform a weight loss study. For an accurate weight loss measure, it was necessary to eliminate the corrosion products that remained on the surface of the samples. The method described by Song et al. [25] was followed. In this method, a chromic solution (100 g/L CrO_3 in distilled water) was used to dissolve the corrosion products.

The tested zones of the samples were put in contact with the chromic solution for 10 minutes. After that time, samples were rinsed with distilled water and dried in air. Then, the final weight of the samples was measured.

3. Results

3.1 Coatings characterization

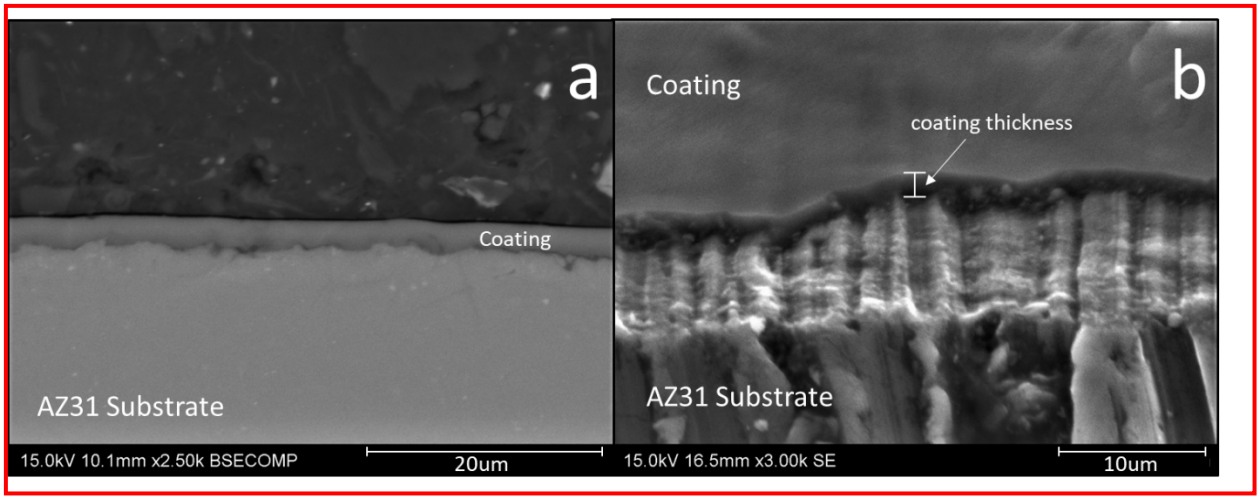

Fig.4. (a) Cross-section view of a SG+SG/CNT multilayer coating. (b) Tilted view of a SG+SG/GNP multilayer coating configuration.

In Fig.4a and Fig.4b a cross-section view of a SG+SG/CNT coating and a 60º tilted view of a SG+SG/GNP coating are shown, respectively. Through a visual assessment previous to the electrochemical test, it was possible to observe that the coatings obtained adhered well to the surface morphology of the substrates and were crack-free. Moreover, it was possible to appreciate that the deposition of these coatings led to a decrease in the surface roughness. The uncoated substrates ground to SiC1200, over which monolayer SG coatings were deposited, showed a roughness value of 0.238 ± 0.04 µm. On the other hand, the monolayer SG coatings over which the second layers for the multilayer coating systems were deposited, showed a roughness value of 0.134 ± 0.02 µm. It was possible to see that the application of the monolayer SG coating lead to a 43.69 % decrease in the roughness value. No cracks were visible in the coatings, and they looked compact and dense. Regarding the nanocharges dispersion, in the case of SG+SG/CNT multilayer coatings, it was possible to observe some MWCNTs aggregates embedded in the coating (Fig.5a and Fig.5b). This was due to the poor dispersion of these unfunctionalized nanocharges. The dispersion states of the GNPs are shown in Fig.5c and

Fig.5d. No COOH-GNPs aggregates were found, and a good dispersion was achieved for the SG+SG/GNP coating systems. The initial concentration of nanocharges for both MWCNTs and COOH-GNPs was 0.005 wt%, but the final nanocharge concentrations in the coatings after the drying and sintering processes were 0.045 wt% and 0.046 wt% for MWCNTs and COOH-GNPs, respectively. These values were calculated based on the proportions of the components in the formulation of the sol-gels and by the evaluation of the volume change after the application of the same heat treatment to a 30 mL volume of both Sol B and Sol C with an equivalent initial nanocharge addition. The initial nanocharge concentration was 0.005 wt% each, as determined from the mass of nanocharges and dilution before the heat treatment. No evaporation of nanocharges was observed during any of the treatments, so the mass of both sols after the heat treatment, along with the mass of the nanocharges incorporated, was used to calculate the final nanocharge concentration after the drying and sintering treatments.

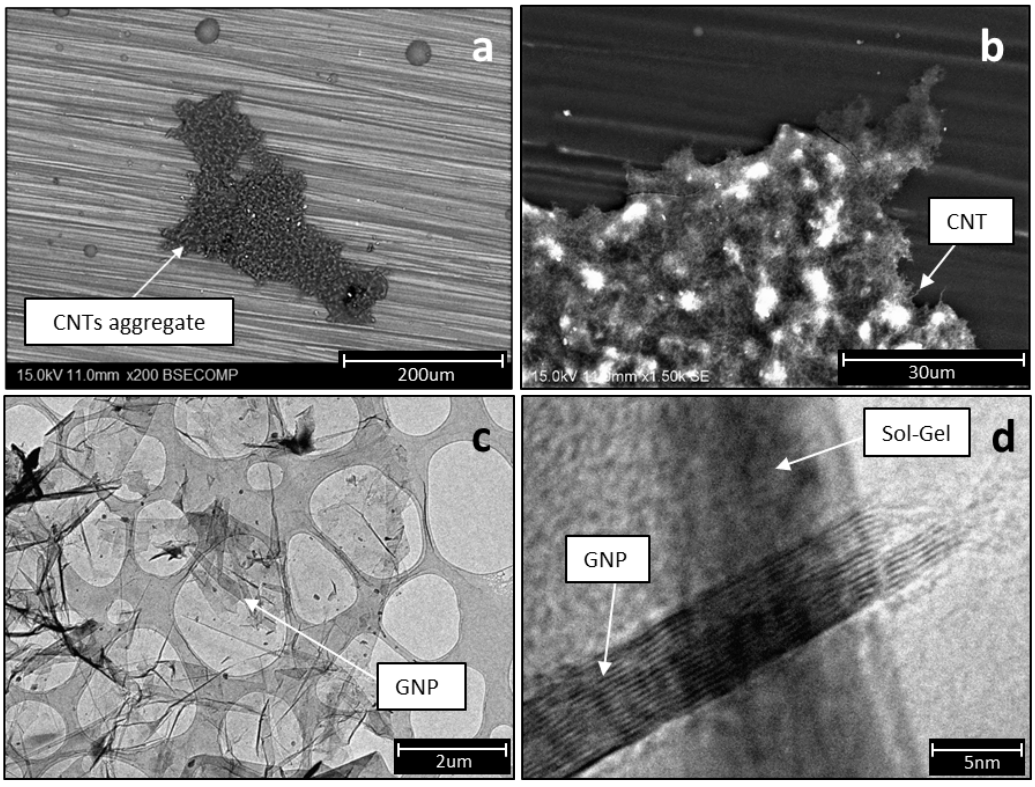

Fig.5. Nanocharge dispersions. (a) MWCNTs aggregate embedded in the sol-gel coating. (b) Detail of MWCNTs aggregate. (c) TEM micrograph of GNPs. (d) GNPs embedded in the sol-gel coating.

Regarding thickness, three different samples were assessed for each coating configuration. The mean thickness values are shown in Fig.6. The thickness values of the multilayer coatings were around 2.2 µm, and no significant differences were found between the three different coating systems. The thickness value of the monolayer coatings was around 1.5 µm.

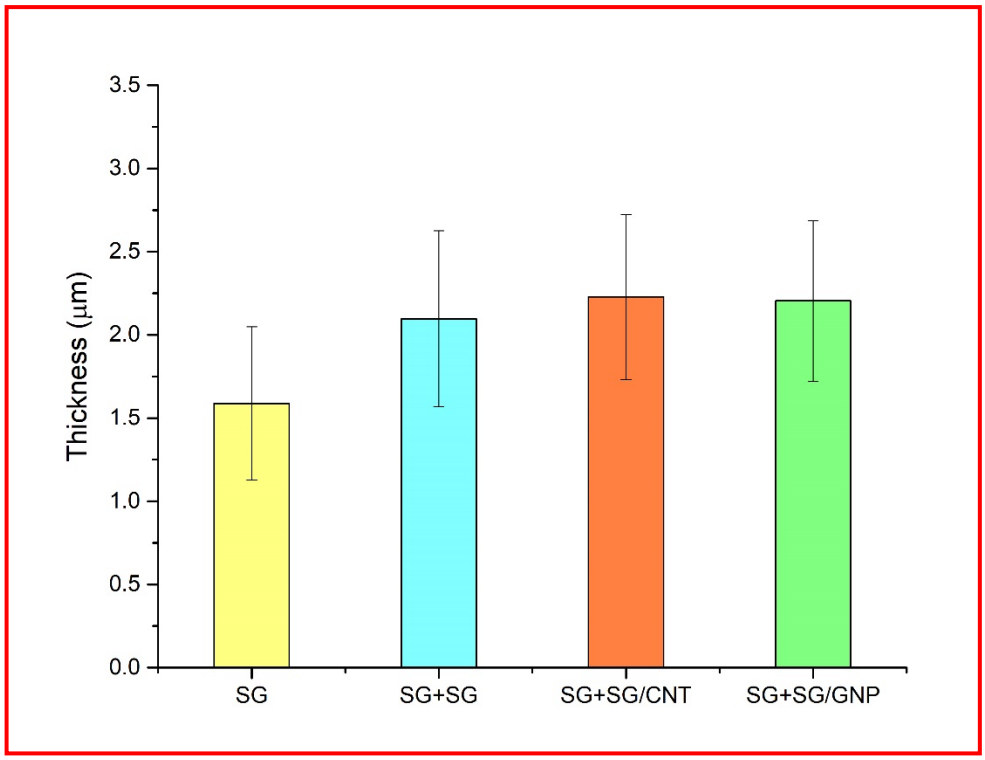

Fig.6. Average coating thickness for the four different coating systems.

In all of the multilayer systems, the coating thickness was higher compared with the monolayer coating system, but actually, the thickness values for the second layers were much lower than expected. This could be a consequence of the reduction of the surface roughness due to the application of a previous coating layer (SG monolayer coating), which showed a far lower roughness value than the uncoated substrate. This implies that the surface roughness of the substrate which is meant to be coated plays an important role in the final thickness of the coating.

3.2 Linear polarization resistance

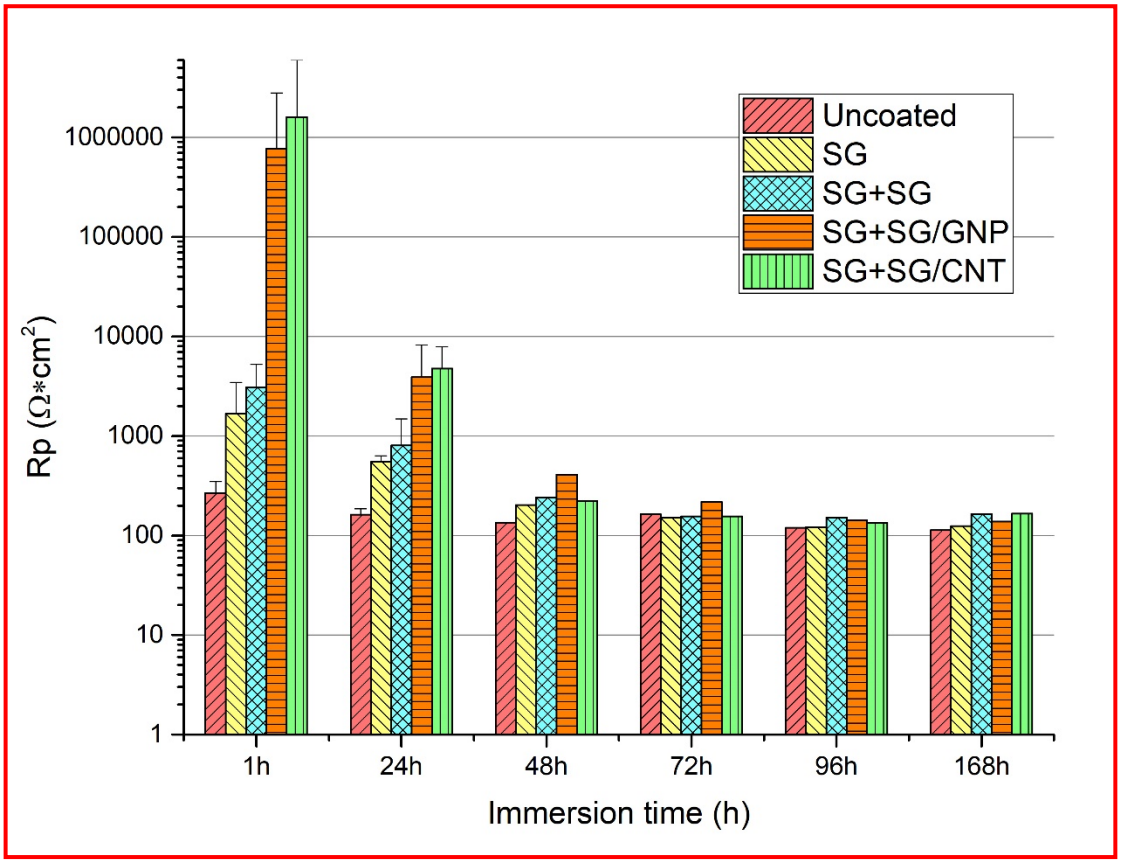

Fig.7. Average linear polarization resistance (*Rp*) values for the different coating systems.

In Fig.7, polarization resistance values are shown for all of the coating systems over 168 hours of immersion. For the first 24 hours of immersion, polarization resistance values of the different coating systems remained higher than the values of the uncoated samples. After 1 hour of immersion, compared with the uncoated samples, the polarization resistance values were one order of magnitude higher in the case of the monolayer SG and the multilayer SG+SG systems, three orders of magnitude higher in the case of the multilayer SG+SG/GNP coating systems and four orders of magnitude higher in the case of the SG+SG/CNT multilayer system. Therefore, the use of the different coating configurations protected the substrates even when they were immersed in a very aggressive medium like 3.5 wt% NaCl solution. However, the polarization resistance values tend to homogenize from 48 hours of immersion onwards. The polarization resistance values of the SG+SG/GNP and SG+SG/CNT configurations are higher

than the values of the other coating systems and the values of the uncoated condition until 24 hours of immersion in the aggressive medium. Therefore, this coating configurations seems to provide the best protection to the substrate against corrosion. The polarization resistance values of the uncoated samples remained almost constant over all of the test. Our results indicate that the $Mg(OH)_2$ coating does not provide any practical protection to the substrate. As it can be observed in Fig.8, the corrosion products layer is cracked and therefore permeable to chlorides present in the NaCl solution. The bad performance of $Mg(OH)_2$ as a passivation layer has been described in previous literature [4]. Moreover, after 48 h of immersion (Fig.8b), the corrosion products layer is thicker, but it appears more cracked and detached than the corrosion products layer after 24 h of immersion (Fig.8a). Another aspect affecting the polarization resistance and the corrosion process is the real area exposed to the medium, which in the case of the uncoated sample, increases when corrosion products crack and detach from the substrate.

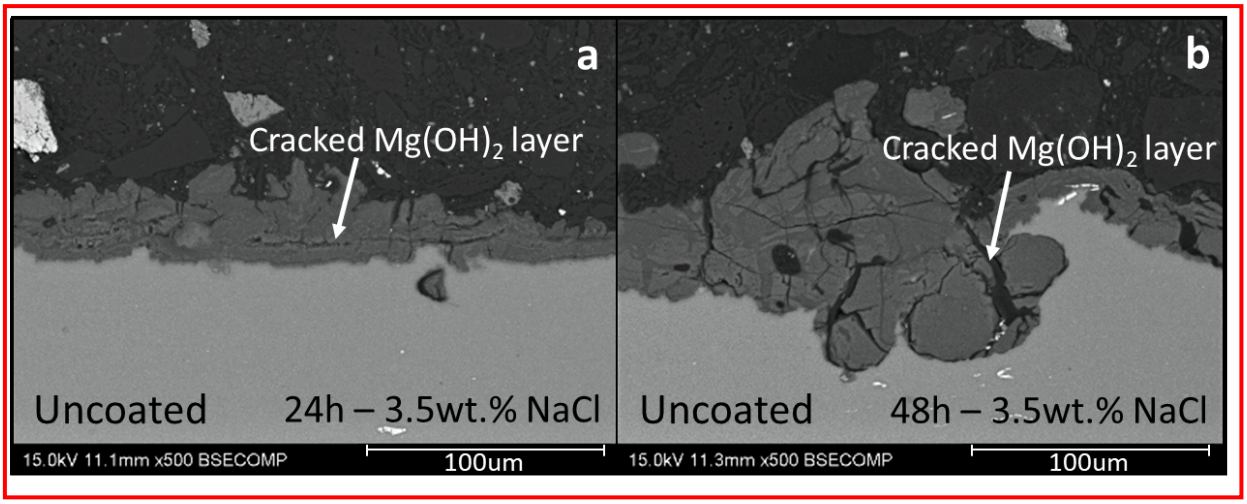

Fig.8. Corrosion products layer on uncoated samples after 24 hours (a) and 48 hours (b) of immersion in 3.5 wt% NaCl solution.

A visual assessment was carried out for the samples until 72 hours of immersion, for longer times all of the samples were corroded (Fig.9). Different samples were used for every coating condition and immersion time. In the case of the uncoated substrate, after 1 hour of immersion, corrosion signs were already visible on the surface of the sample. For the same immersion time, no corrosion signs were visible for any coated sample.

From 24 hours of immersion onwards, the tested area of the uncoated condition is totally corroded and damaged. On the other hand, for all the coated conditions, there is no evident sign of pitting or generalized corrosion process in the tested zone, which reveals the effective corrosion protection of the different coating configurations. However, it is possible to appreciate some corrosion signs, mainly localized at the edge of the tested area in contact with the plastic O-ring used for sealing the immersion zone, where crevice corrosion may take place. The actual corrosion attack depth is lower for the SG coating configuration.

It is important to emphasize that a 3.5 wt% NaCl solution is a very aggressive medium, especially for a low corrosion-resistant metal like magnesium.

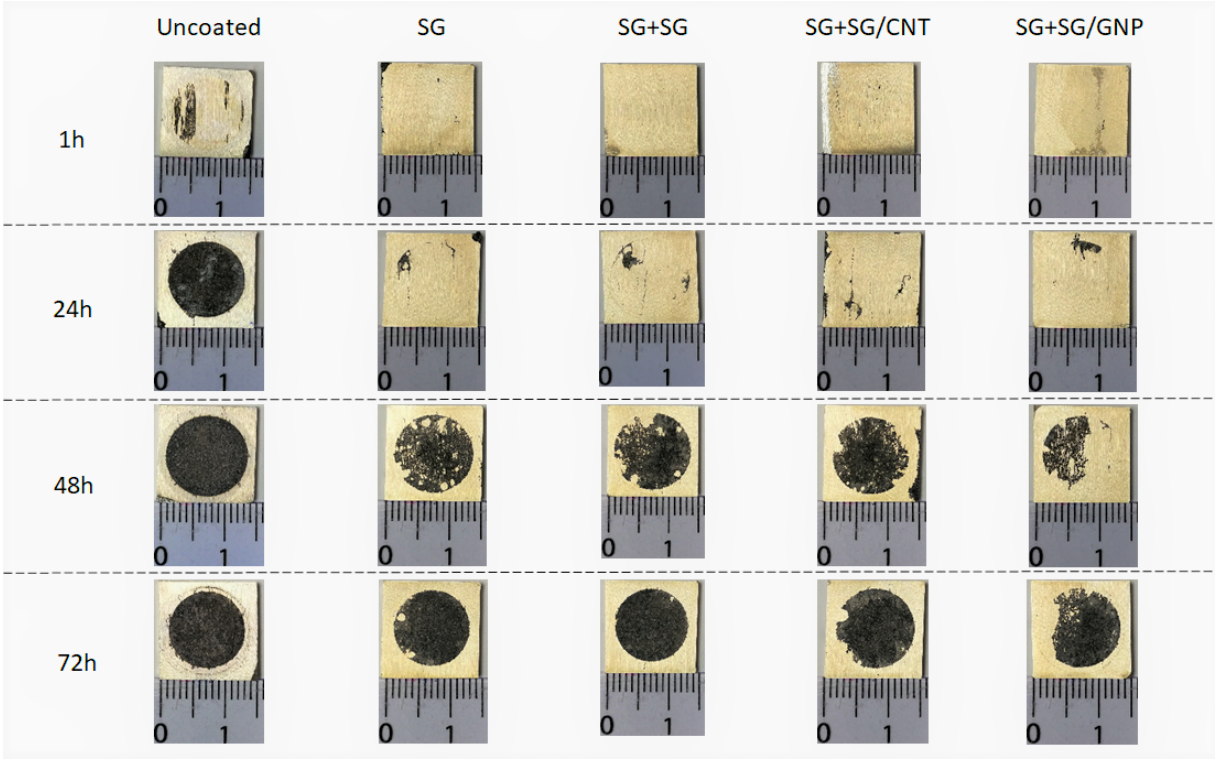

Fig.9. Evolution of the corrosion process over 72 hours of immersion in 3.5 wt% NaCl medium for all the coating configurations.

3.3 Anodic-cathodic polarization tests (Tafel)

Anodic-cathodic tests were carried out for two different immersion times, 1 hour (Fig.10a) and 24 hours (Fig.10b) of immersion in 3.5 wt% NaCl solution. The collected data are shown in Table 2.

Table 2. Electrochemical corrosion data extracted from anodic-cathodic polarization tests.

	Ecorr (V)		Current density (A/cm^2)	
	1h	24h	1h	24h
Uncoated	-1.41	-1.31	3.5 x 10^{-6}	6.6 x 10^{-6}
SG	-1.45	-1.38	1.9 x 10^{-7}	1.2 x 10^{-6}
SG+SG	-1.46	-1.32	1.1 x 10^{-7}	7.6 x 10^{-7}
SG+SG/CNT	-1.44	-1.36	2.9 x 10^{-8}	4.9 x 10^{-7}
SG+SG/GNP	-1.42	-1.39	2.5 x 10^{-7}	5.2 x 10^{-7}

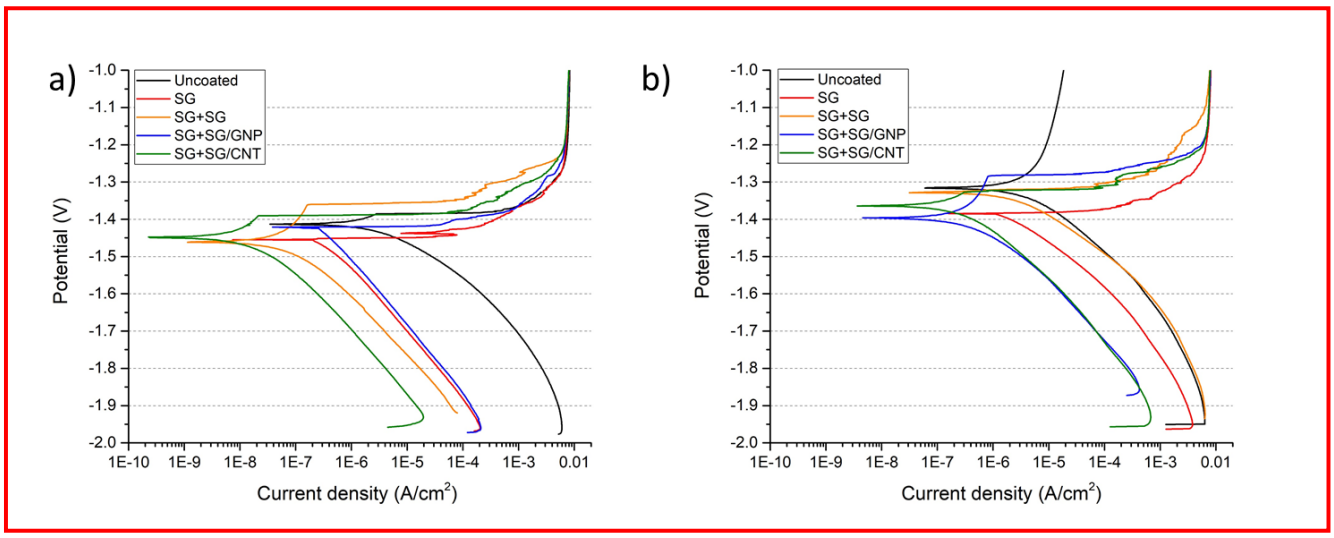

Fig.10. Anodic-cathodic polarization curves for 1 hour (a) and 24 hours (b) of immersion in 3.5 wt% NaCl.

The current density values were calculated according to the method proposed by Stern and Geary [24][26]. In this method, corrosion density is calculated from the polarization resistance (*Rp*) and the proportionality constant B, whose value depends on the slopes of the anodic (b_a) and cathodic (b_c) curves of the anodic-cathodic plots, as shown in equations (1) and (2):

$$i_{corr} = \frac{B}{Rp} \quad (1)$$

$$B = \frac{|b_a||b_c|}{2.3(|b_a| + |b_c|)} \quad (2)$$

All of the data were obtained with the implementation of equations (1) and (2) in the software Nova 2.1 provided by Metrohm Autolab, which was used to carry out the electrochemical tests and to calculate the polarization resistance and current density values.

After 1 hour of immersion, all of the E_{corr} potential values vary between -1.41 V for the uncoated sample and -1.46 V for the SG+SG configuration, which have the most electronegative potential. Related to current density, the uncoated sample shows the highest value which are one order of magnitude higher than values of the SG, SG+SG and SG+SG/GNP configurations and two orders of magnitude higher than the current density of the SG+SG/CNT configuration. Moreover, in the case of the SG and SG+SG/GNP coating systems, the pitting potential is below the corrosion potential. The SG+SG/CNT coating configuration provides the best corrosion protection after 1 hour of immersion in 3.5 wt% NaCl.

After 24 hours of immersion, E_{corr} potential turned less electronegative for all samples. All of the E_{corr} potential values vary between -1.31 V for the uncoated sample and -1.39 V for the SG+SG/GNP configuration, which have the most electronegative potential. Regarding current density after 24h of immersion, the uncoated sample shows the highest value, 6.6E-06 A/cm^2. The monolayer SG configuration has a current density value in the same order of magnitude than the value for the uncoated sample, 1.2E-06 A/cm^2, but lower than that. The multilayer SG+SG, SG+SG/CNT and SG+SG/GNP systems show the lowest values, 7.6E-07 A/cm^2, 4.9E-07 A/cm2 and 5.2E-07 A/cm^2 respectively, which are one order of magnitude lower than the value of the uncoated substrate. Therefore, the multilayer coating configurations provide an improvement against corrosion compared to uncoated substrates.

Looking at the anodic-cathodic plots, the pitting potential is below the corrosion potential for some of the samples. It is important to note that the use of magnesium as substrate could lead to limitations during the electrochemical tests due to the Negative Difference Effect (NDE) that takes place in magnesium alloys. Due to this effect, an estimation of the current density based on the polarization curves is imprecise, because the reaction mechanism around the corrosion potential induce changes in the polarization curves, even exhibiting linear regions in some cases. Thus, the polarization curves may not be a reliable method to estimate the corrosion rate of magnesium and magnesium alloys [25][27]. However, the multilayer coating configurations perform an improvement against corrosion compared to uncoated substrates.

3.4 Hydrogen evolution

The results of the H_2 volume evolution for every condition are shown in Fig.11. All of the different coating configurations improved the behaviour against corrosion compared with the uncoated condition, reducing the final volume of evolved H_2 after 168h of immersion in a very aggressive medium like 3.5 wt% NaCl. From the beginning of the experiment, the SG+SG multilayer system shows higher values of evolved H_2 than all of the other coating systems, but it was still lower than the values of the uncoated sample. However, the SG+SG system behaves in a more linear way than all of the other systems, and at the end of the experiment, the final volume of evolved H_2 is similar to the values of SG and SG+SG/GNP coating configurations. Within the first 24 hours, the multilayer SG+SG/CNT system presents the lowest value of evolved H_2. This is coherent with the data obtained by the electrochemical tests where SG+SG/CNT coatings showed the best corrosion protection for 24 hours of immersion.

However, at the end of the experiment, the SG+SG/GNP system, with a final volume of 15.42 mL/cm^2, and the SG system, with an evolved volume of 15.96 mL/cm^2, achieve a volume reduction of 49 % and 47 %, respectively, when compared with the uncoated sample, and these were the lowest values of evolved H_2. In the case of the SG+SG coating system, the final

volume of evolved H_2 is 17.37 mL/cm^2, which means a reduction of 42 % compared to the uncoated substrate. Finally, for the SG+SG/CNT coating, the volume reduction of evolved H_2 (with a value of 28 %) compared with that of the uncoated sample is lower than the other coating configurations.

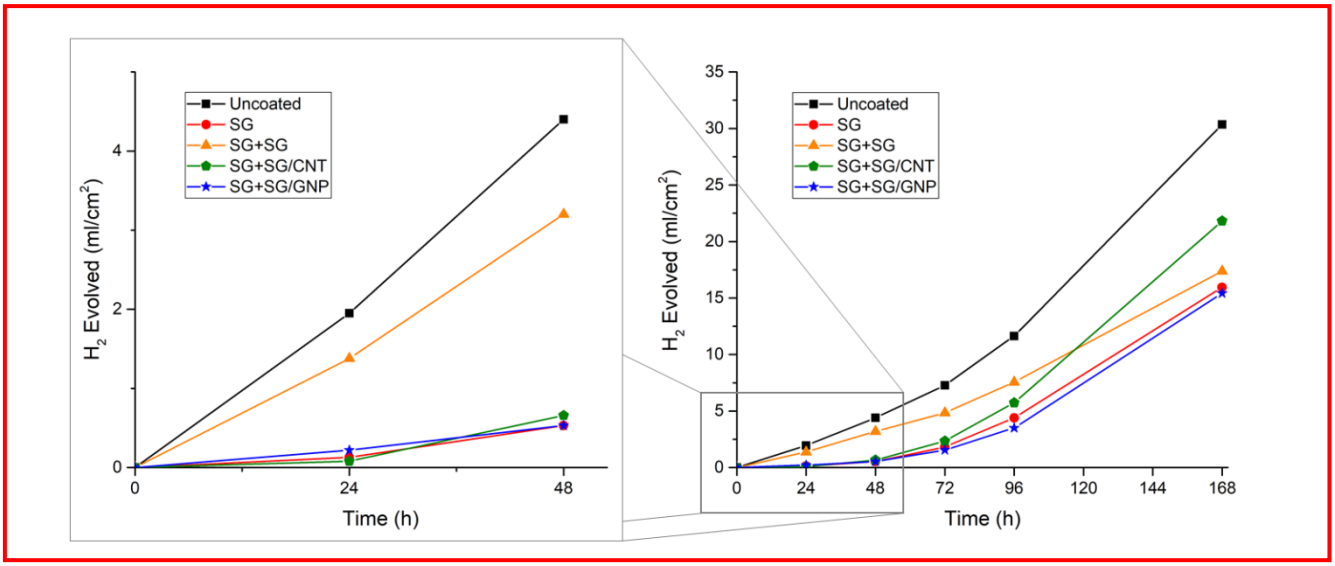

Fig.11. H_2 evolution test for 168 h of immersion in 3.5 wt% NaCl and detail of the first 48 h of immersion.

3.5 Gravimetric test

After the hydrogen evolution tests, a gravimetric study was carried out to obtain information about the corrosion rate for the different conditions. To perform an accurate measure, the corrosion products on the surface of the samples were removed using the method described by Song et al. [25] The values of the corrosion rates for the different coating systems are shown in Fig.12. As expected from the H_2 evolution tests, all of the coating configurations provided an improvement in the behaviour against corrosion in the gravimetric test. The uncoated sample had the highest corrosion rate value, 3.714 mg/cm^2/day. After immersed for 168h in 3.5 wt% NaCl solution, the SG coating with 1.943 mg/cm^2/day and the SG+SG/GNP system with 2.21 mg/cm^2/day had the lowest corrosion rate values, achieving a reduction in the corrosion rate of about 47 % and 40 % respectively. This is a significant result taking into account the aggressive

medium used to carry out the test. The SG+SG system had a corrosion rate value of 2.324 mg/cm^2/day which means a reduction of corrosion rate of about 37 % compared to the uncoated sample. Finally, as in the H_2 evolution tests, after 168 h of immersion in 3.5 wt% NaCl, the SG+SG/CNT coating configuration shows the highest corrosion rate of all coating configurations, with a value of 3.029 mg/cm^2/day. This coating configuration achieved a reduction of about 18 % of the corrosion rate compared to the uncoated substrate, which is still a good result.

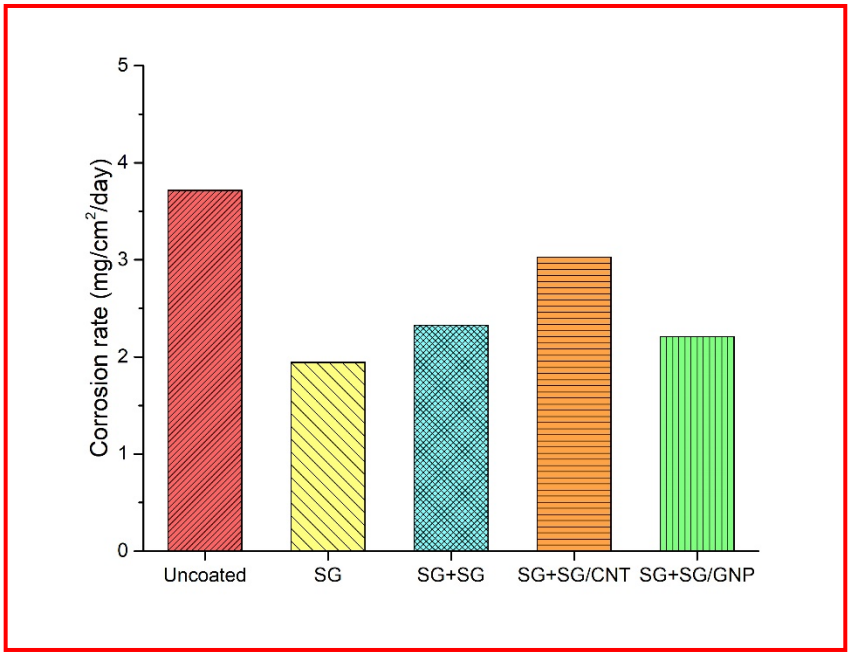

Fig.12. Corrosion rate of the Mg alloy coated with the different coating systems after 168 h of immersion in 3.5 wt% NaCl.

Fig.13 shows the surfaces of the different samples after removal of the corrosion products. In the colour diagrams, it is possible to appreciate that the depth of the damage was far greater for the uncoated sample than for the coated samples. The difference between the lowest and the highest points of the surface of the uncoated sample was around 650 µm. For the coated samples, the depth of the corrosion was around 280 µm for the SG coating, 370 µm for the SG+SG coating, 500 µm for the SG+SG/CNT coating, and finally 340 µm for the SG+SG/GNP coating configuration.

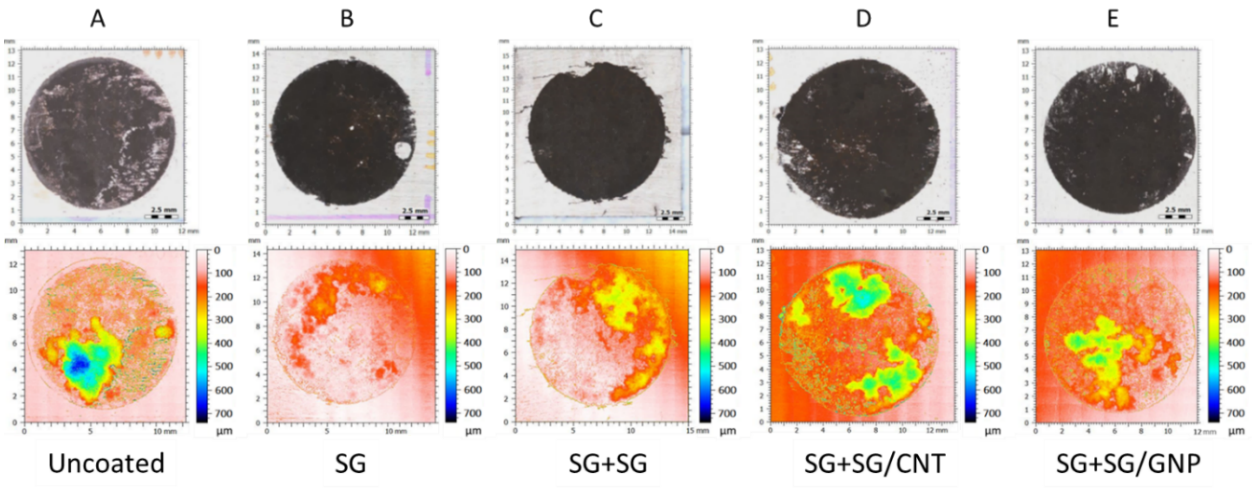

Fig.13. Corrosion prints after 168 h of immersion of the different coating systems: (a) Uncoated, (b) SG, (c) SG+SG, (d) SG+SG/CNT, (e) SG+SG/GNP.

According to corrosion rates from the gravimetric test after 168 hours of experiment, the lowest values belong to the SG and SG+SG/GNP coatings, which also have the lowest value of corrosion depth, indicating the better corrosion performance of these two coating systems for a long testing period in such an aggressive environment, i.e., 3.5 wt% NaCl aqueous solution.

4. Discussion

To establish a comparative frame to assess the anticorrosion behaviour of the different coating systems developed in this research, especially the multilayer systems doped with carbon nanotubes and graphene nanoplatelets, the results of the anodic-cathodic tests were compared with some results found in the literature. López et al. [23] used single layer sol-gel silica coatings for corrosion protection of ZE41 magnesium alloy. After 1h of immersion in 3.5 wt% NaCl, the lowest current density value obtained was $7.9 \cdot 10^{-6}$ A/cm^2. This current density value is between one and two orders of magnitude higher than the values obtained in our research for the different coating systems, despite the lower corrosion resistance of the AZ31 alloys used in this work. M. Zaharescu et al. [28] used SiO_2 based hybrid inorganic-organic mono- and bi-layer sol-gel coatings doped with TiO_2-CeO_2 nanoparticles for corrosion protection of AZ31B magnesium alloy. After 30 min of immersion in 0.3 wt% NaCl solution, the current density

values for the monolayer and the bilayer coatings were in the order of 10^{-7} A/cm^2 and 10^{-6} A/cm^2, respectively. However, in the present research, the lowest current density values after 24 h of immersion in 3.5 wt% NaCl for the SG+SG/CNT and the SG+SG/GNP coating systems were in the same order of magnitude: $4.9 \cdot 10^{-7}$ A/cm^2 and $5.2 \cdot 10^{-7}$ A/cm^2 respectively, but for longer immersion time and with higher chloride concentration in the electrolyte (3.5 wt% NaCl).

As seen in Fig.9, for immersion times longer than 72 hours, the surfaces of all samples were totally damaged and corroded. Therefore, micrographs were taken for samples immersed in 3.5 wt% NaCl solution for 48 hours at most. SEM cross-section micrographs were taken to determine the corrosion mechanisms that took place in the different coating configurations during corrosion tests. The cross-section view of the uncoated samples after 1 hour, 24 hours and 48 hours of immersion in a 3.5 wt% NaCl solution (Fig.14a – Fig.14c) revealed the progression of the formation of a corrosion products layer during the corrosion process. After 1 hour (Fig.14a), the corrosion products layer reached a thickness value of around 10 μm. At this time, the corrosion was uniform and generalized on all of the surface, and deeper pitting corrosion mechanisms were also visible. After 24 hours of immersion (Fig.14b), the thickness of the corrosion products layer reached values of around 30 μm. The corrosion was generalized on the whole surface. Finally, after 48 hours of immersion (Fig.14c), the thickness of the corrosion products layer reached values of around 50 μm and in certain zones, this value was even higher than 100 μm. There were signs that generalized and pitting corrosion were the mechanisms that took place for these samples.

The cross-section images of the monolayer SG coatings show the degradation process during the first 48 hours of immersion (Fig.14d – Fig.14f). After 1 hour (Fig.14d), the coating thickness value was around 1.5 μm, the same thickness shown in Fig.6 for this coating configuration, and no corrosion signs were visible. After 24 hours (Fig.14e), corrosion signs appeared in the zones where the coating was damaged. At these breaking points, corrosion started to spread under the

coating, between the coating-substrate interface. This was due to a crevice corrosion mechanism. After 48 hours of immersion (Fig.14f), some parts of the coating were totally detached and cracked, and corrosion was generalized on the surface of the substrate.

Fig.14g – Fig.14i show the corrosion process for the multilayer SG+SG coating system during the first 48 hours of immersion. After 1 hour (Fig.14g), the coating thickness value was around 2 μm, the same thickness shown in Fig.6 for this coating configuration. There were cracks in the coating but no corrosion signs were found for this immersion time. After 24 hours (Fig.14h), the corrosion process was initiated in the zones where the coating was detached. Finally, after 48 hours of immersion (Fig.14i), the coating was totally detached and corrosion was generalized.

The cross-section images of the multilayer SG+SG/CNT coating system (Fig.14j – Fig.14l) show the degradation process during the first 48 hours of immersion. After 1 hour (Fig.14j), the coating had a thickness value of around 2 μm, the same thickness shown in Fig.6 for this coating configuration. The coating remained attached to the surface and without cracks. After 24 hours (Fig.14k), the coating was slightly thinner and detached. Cracks were visible. At this time, crevice corrosion was found spreading between the detached coating and the substrate. After 48 hours of immersion (Fig.14l), the coating was missing and the corrosion was generalized.

Finally, the corrosion process during 48 hours for the multilayer SG+SG/GNP coating configuration is shown for Fig.14m – Fig.14o. After 1 hour (Fig.14m), no signs of corrosion were visible and the coating had a thickness value of around 2 μm, the same thickness shown in Fig.6 for this coating system. After 24 hours of immersion (Fig.14n), the coating remained attached and without cracks, and no corrosion signs were visible in the assessed area. After 48 hours (Fig.14o), the coating was still present in some zones, but it was cracked and detached in other parts, and the crevice corrosion mechanism started to spread between the detached coating and the surface of the substrate. With this coating configuration, the beginning of the corrosion

process was delayed in comparison with the other coating systems, therefore the corrosion products layer on these samples after 48 hours of immersion was thinner than in the previous cases.

For all of the different coating systems, the barrier effect to protect the substrates against corrosion was successfully achieved. The images demonstrate that, for the coated conditions, the corrosion processes began between 24 and 48 hours after the immersion in 3.5 wt% NaCl, but for the uncoated samples, the corrosion process was instantaneous. The multilayer SG+SG/GNP coating system shows the best anticorrosion behaviour.

For a better understanding of how coatings broke and then corrosion processes were initiated, plain-view micrographs were taken of the surface of the damaged coatings. Fig.15a shows a breaking point of the coating. These points appeared as a result of the presence of cracks or defects in the coating and were the starting points for the corrosion process of the substrate. Once the aggressive medium reached the substrate, the corrosion process was initiated. Then, the corrosion products spread radially between the substrate-coating interface due to the formation of a differential aeration cell, which promoted crevice (Fig.15a) and filiform (Fig.15b) corrosion mechanisms. In Fig.15a is possible to see a darker area surrounding the breaking point, marked with arrows, which corresponds with the spread of corrosion products under the coating. In Fig.15b, the corrosion products spread between the coating and the substrate with a filiform corrosion morphology.

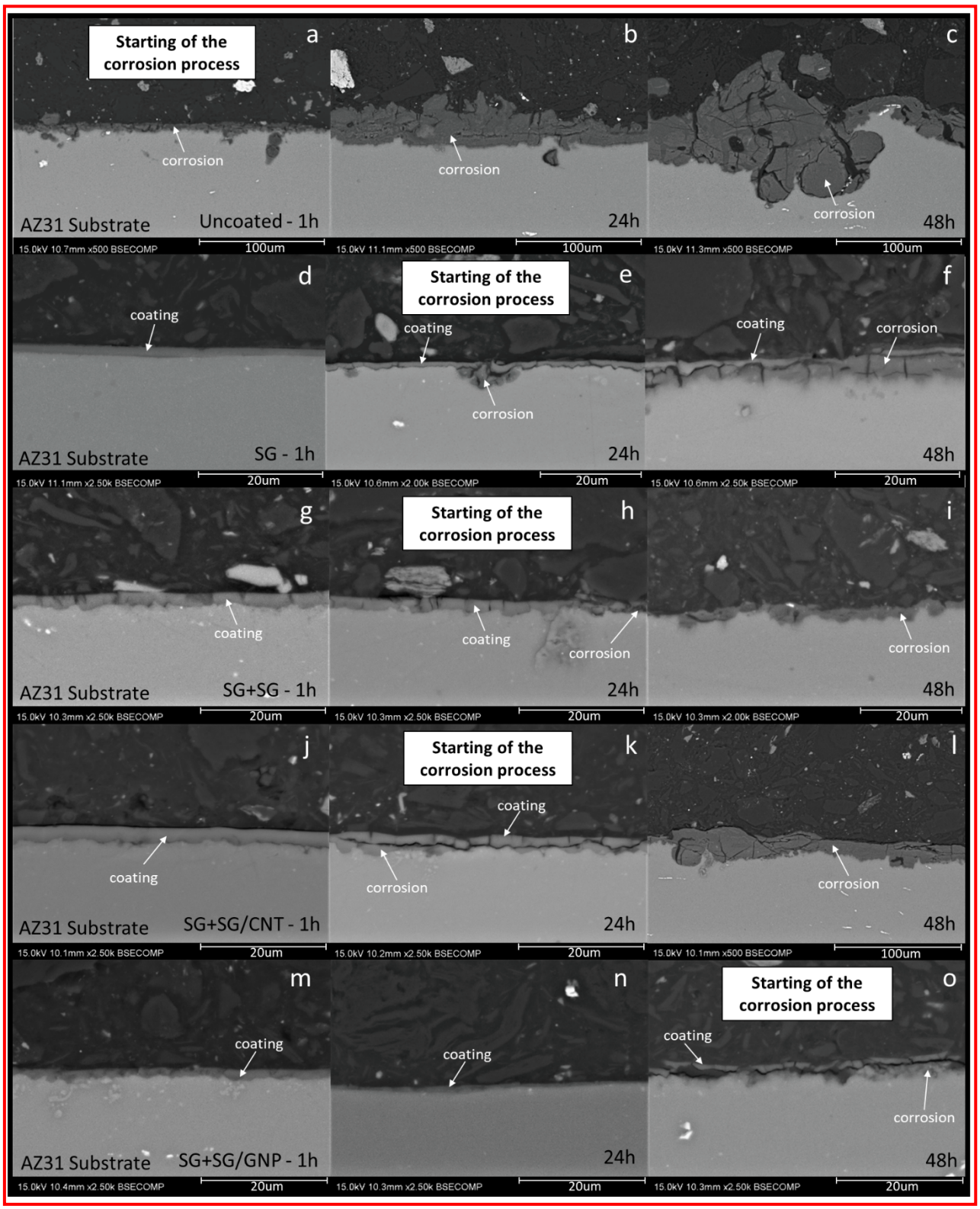

Fig.14. Cross-section micrographs of the progression of the corrosion process for all of the tested samples: (a) Uncoated, 1 hour of immersion. (b) Uncoated, 24 hours of immersion. (c) Uncoated, 48 hours of immersion. (d) SG, 1 hour of immersion. (e) SG, 24 hours of immersion. (f) SG, 48 hours of immersion. (g) SG+SG, 1 hour of immersion. (h) SG+SG, 24

hours of immersion. (i) SG+SG, 48 hours of immersion. (j) SG+SG/CNT, 1 hour of immersion. (k) SG+SG/CNT, 24 hours of immersion. (l) SG+SG/CNT, 48 hours of immersion. (m) SG+SG/GNP, 1 hour of immersion. (n) SG+SG/GNP, 24 hours of immersion. (o) SG+SG/GNP, 48 hours of immersion.

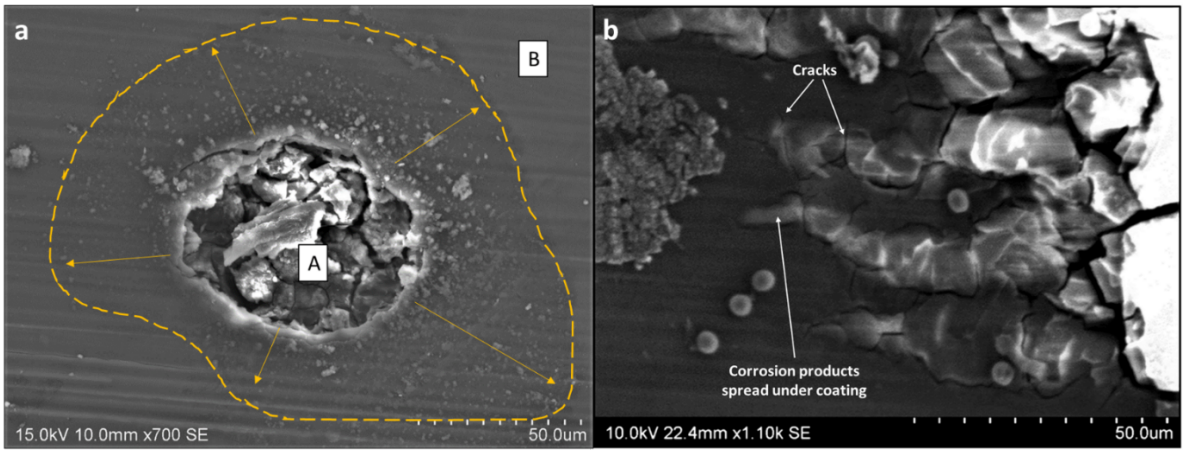

Fig.15. (a) Corrosion breaking point in a monolayer SG coating configuration. (b) Corrosion products spreading in the interface between the substrate and the SG monolayer coating.

The formation and the increase in the volume of the corrosion products in the coating-substrate interface caused the cracking and detachment of the coating. As seen in Fig.14, once the coating was totally detached from the substrate, the corrosion was generalized. An EDX assessment was carried out to study the composition inside and outside of one of these circular breaking points (Fig.16). This study shows that in the zone marked as A in Fig.15a magnesium oxides were formed and negligible traces of silicon from the coating were detected (Fig.16a). However, outside the circular morphology, the coating still remains without damage, as can be seen in the zone marked as B in Fig.15a. In this zone, silicon is detected as well as oxygen, this oxygen is part of the SiO_2 coating. Moreover, due to the low thickness of the coating, magnesium from the substrate is also detected in this zone (Fig.16b).

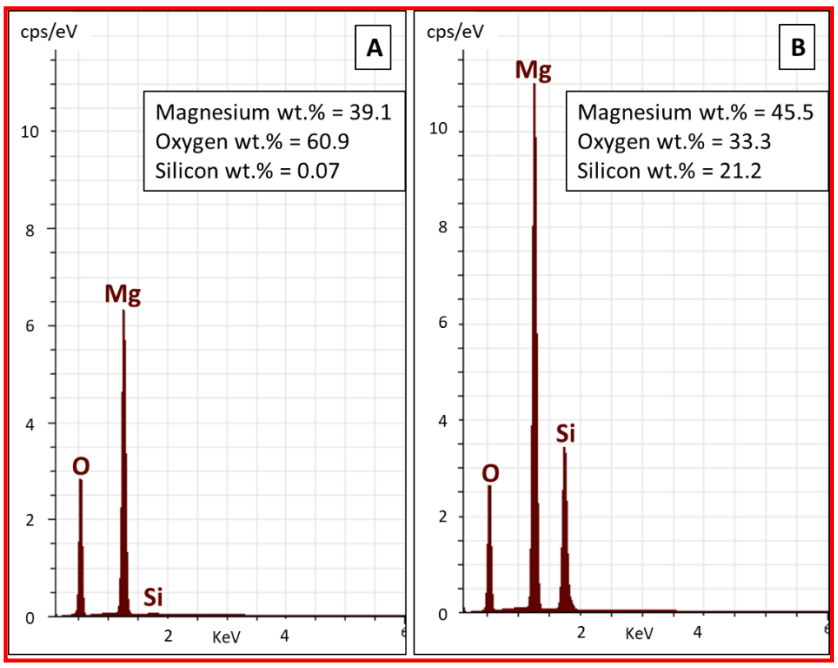

Fig.16. (a) EDX in the zone marked as A in Fig 14. (b) EDX in the zone marked as B in Fig 14.

Regarding the different coating systems, no cracks were observed in coatings previous to electrochemical tests, but even after the electrochemical test, some detached parts of the coatings were not totally cracked and broken (Fig.14e, Fig.14f, Fig.14k). As expected, this indicates that the combination of inorganic and organic precursors gave hybrid sol-gel coatings which are less brittle than pure inorganic or pure organic coatings.

Based on all of the electrochemical tests, the visual evaluation of the tested areas, and the cross-section micrographs, it is possible to affirm that the presence of the different coating systems improved the behaviour against corrosion of the coated substrates, acting as an effective physical barrier against corrosion processes. In the polarization resistance test, the multilayer SG+SG/GNP and the SG+SG/CNT coating systems showed the highest polarization resistance values until 24 hours of immersion in 3.5 wt% NaCl solution, (Fig.7). Over the first 24 hours of immersion, the SG+SG/GNP coating remained attached and without cracks (Fig.14n). However, after 48 hours of immersion, generalized corrosion was present in all of the different samples, but at this time, the corrosion process was at its initial stage for the SG+SG/GNP

coating system, and the coating was detached but still present on the sample. Moreover, the corroded area of the substrate coated with the SG+SG/GNP multilayer system was smaller than the affected areas for all the other coating conditions, as it can be seen in Fig.9.

The current density values for all of the different conditons increased from 1 hour of immersion until 24 hours of immersion in 3.5 wt% NaCl. Over the first 24 hours, the multilayer systems provided the best protection against corrosion. for the SG+SG/GNP multilayer system, the coating remained attached and no significant corrosion signs were visible after 24 hours of immersion (Fig.14n). In the case of SG+SG/CNT and SG+SG/GNP multilayer systems, signs of a pitting corrosion mechanism were visible in the anodic-cathodic curves at 24 hours of immersion in 3.5 wt% NaCl.

Regarding the hydrogen evolution tests. From the beginning, the SG+SG multilayer system was cracked (Fig.14g). This might have occurred because, without any kind of nano-reinforcement, the thickness achieved was too high to obtain coatings without cracks, because of the tensions generated during the thermal treatment of the coatings [29]. Moreover, for a sol-gel synthesized from TEOS and MTES with an MTES content of 60% (molar fraction TEOS/MTES:40%/60%), Innocenzi et al. [13] reported that the critical coating thickness was around 2 μm, which matches with the mean thickness value of the SG+SG multilayer coating system developed in this work. This means that the critical thickness was achieved and the lack of nano-reinforcement in this coating system caused cracks to appear. The substrate under these cracks could be the starting points for pitting corrosion mechanisms. This would result in higher values of evolved hydrogen, compared with the other coating systems. Corrosion products growing inside the cracks of the SG+SG coating system as a result of pitting corrosion could help to temporarily isolate the substrate from the aggressive media, reducing the hydrogen evolution at these points, while the multilayer coating was degrading in other zones where generalized corrosion was taking place. This mechanism could be present until 48 hours after immersion when the coating disappeared and the corrosion was generalized (Fig.14i). Looking

at Fig.11, the hydrogen evolution for the SG+SG system had a linear behaviour until 72 hours when hydrogen evolution started to increase faster due to the lack of coating and the generalized corrosion mechanism. For the first 48 hours of immersion, the SG+SG/CNT multilayer coating behaved similar to the monolayer SG and the multilayer SG+SG/GNP systems. However, unlike these other coating systems, after 48 hours of immersion, the SG+SG/CNT coating was missing, the corrosion was generalized, and the corrosion products layer showed a significant thickness (Fig.14l). From that moment, the hydrogen evolution increased faster than in the other cases. The poor dispersion of the MWCNTs could explain why these nanocharges were not acting as an effective nano-reinforcement. Also, this could explain the early presence of cracks in this coating system (Fig.14k). Finally, the lowest values of evolved hydrogen were achieved in the case of the monolayer SG and the multilayer SG+SG/GNP coating systems. While it is true that the SG monolayer system was not reinforced with any kind of nanocharges, the lower thickness value of this coating avoided the early presence of cracks, contrary to what happened to SG+SG multilayer system. Thus, this coating was able to preserve its protective properties for a longer time. In the case of the SG+SG/GNP multilayer coating, the thickness was higher, but the dispersion of the nanocharges was effectively achieved in this case, and the coating provided its protective properties against corrosion for a longer time.

The better performance of the doped multilayer coating configurations compared with the multilayer SG+SG coating system could be a consequence of the properties that these nanocharges provide to the coatings. As described in the literature, the use of carbon nanotubes could help to maintain the integrity of the coating, making it more resistant and durable through the bridging mechanism [18]. However, due to the poor dispersion of the MWCNTs, this mechanism was not likely to take place. At the same time, the use of graphene nanoplatelets could make it more difficult for the chloride ions of the aggressive medium to pass through the coating to reach the substrate surface, making it more resistant and durable against corrosion [16].

After all of these considerations, the proposed corrosion mechanism that has taken place in the coated samples is exposed in Fig.17. At first, the presence of the sol-gel coating prevents the water molecules from reaching the surface of the magnesium substrate. However, the chloride ions present in the medium can pass through the coating, attack the surface, and promote the formation of an increased volume of corrosion products that breaks the coating and exposes the substrate to the medium. Once the substrate is exposed, the water molecules present in the medium can reach the surface and the corrosion process is promoted. Magnesium hydroxide is formed as a product of the corrosion reaction of the magnesium substrate. The corrosion products begin to spread and grow between the coating-substrate interface, and this leads to further cracking and detaching the coating above. Once the coating is detached, more water molecules can reach the substrate and the corrosion process starts over again.

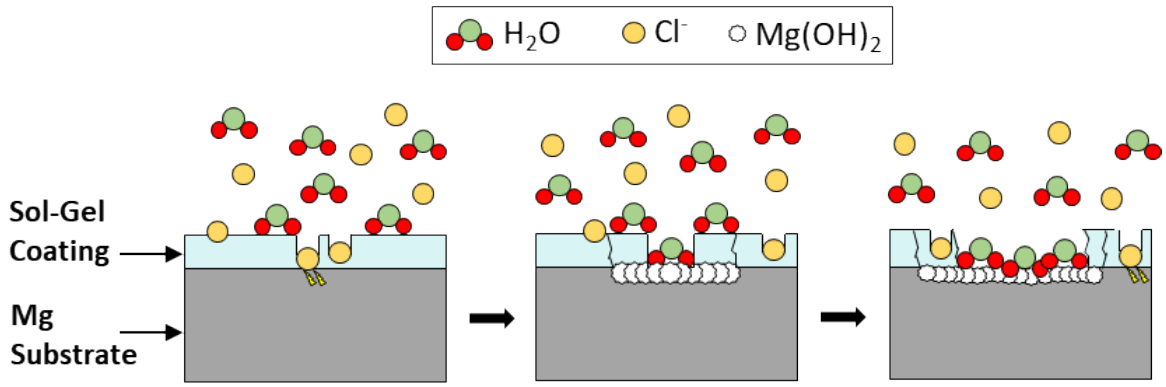

Fig.17. Coating degradation and substrate corrosion mechanism scheme.

5. Conclusions

A combination of sol-gel synthesis and the dip-coating method were used to generate compact, homogeneous, crack-free and thickness-controlled hybrid silica coatings on the surface of light alloys like the AZ31B magnesium alloy. Coatings with a thickness of about 2 µm were obtained. Multilayer coatings were about 30 % thicker than monolayer coatings and the multilayer coatings doped with nanocharges (MWCNTs and COOH-GNPs) achieved the highest thickness values.

The multilayer SG+SG/CNT coating systems did not perform as well as expected. This has been associated with poor nanocharge dispersion due to the use of non-functionalized MWCNTs. Therefore, it would be interesting to use functionalized MWCNTs in the future, which could improve the anticorrosion properties of the SG+SG/CNT multilayer coating systems.

For the first 24 hours of immersion, which was the time for which the coatings performed their best protective behaviour in 3.5 wt% NaCl medium, the multilayer SG+SG/GNP coating configuration showed one of the highest values of polarization resistance, one of the lowest values of current density, and after 168 hours of immersion, this coating configuration shows the lowest value of evolved hydrogen, almost 50 % less evolved hydrogen compared to the uncoated substrate. Therefore, the multilayer SG+SG/GNP coating system provided significant protection against corrosion, and it is an excellent candidate for further research.

The order of the different coating systems based on their better anticorrosion protective properties is as follows: SG+SG/GNP showed the best anticorrosion behaviour, from the electrochemical tests, the hydrogen evolution tests and the SEM assessment. The presence of COOH-GNPs let to an increase in the toughness of the coating and made it more difficult for the chloride ions to reach the surface of the substrate, delaying the starting of the corrosive process. Then, the multilayer SG+SG/CNT coating system showed a good anticorrosion behavior for the first 24 hours of immersion in the 3.5 wt% NaCl medium. However, for longer immersion times the performance of this coating system decreases. The poor dispersion of the nanocharges and the formation of MWCNT agglomerates was counterproductive to achieving a better anticorrosion protective coating. The use of functionalized CNTs could improve the anticorrosion properties of this coating system. The next coating system is the multilayer

SG+SG which was too thick to remain crack-free after the thermal treatment, taking into account that this coating system did not have any nano-reinforcement. Finally, the monolayer SG coating systems were thinner but also showed an improvement against corrosion. All of the coating configurations improved the behaviour against corrosion compared to the uncoated AZ31 substrate.

Acknowledgment

The authors would like to acknowledge Ministerio de Ciencia e Innovación (FPI grant BES-2016-076946), Agencia Estatal de Investigación (RTI 2018-0963-B-C31) and Comunidad de Madrid Project ADITIMAT-CM (S2018/NMT-4411) for their economic support.

References

[1] B.L. Mordike, T. Ebert, Magnesium Properties - applications - potential, Mater. Sci. Eng. A. 302 (2001) 37–45. https://doi.org/10.1016/S0921-5093(00)01351-4.

[2] R.G. Hu, S. Zhang, J.F. Bu, C.J. Lin, G.L. Song, Recent progress in corrosion protection of magnesium alloys by organic coatings, Prog. Org. Coatings. 73 (2012) 129–141. https://doi.org/10.1016/j.porgcoat.2011.10.011.

[3] G. Song, Recent progress in corrosion and protection of magnesium alloys, Adv. Eng. Mater. 7 (2005) 563–586. https://doi.org/10.1002/adem.200500013.

[4] G.L. Song, A. Atrens, Corrosion mechanisms of magnesium alloys, Adv. Eng. Mater. 1 (1999) 11–33. https://doi.org/10.1002/(SICI)1527-2648(199909)1:1<11::AID-ADEM11>3.0.CO;2-N.

[5] G. Song, A. Atrens, Understanding magnesium corrosion. A framework for improved alloy performance, Adv. Eng. Mater. 5 (2003) 837–858. https://doi.org/10.1002/adem.200310405.

[6] M. Atik, P. de Lima Neto, L.A. Avaca, M.A. Aegerter, Sol-gel thin films for corrosion protection, Ceram. Int. 21 (1995) 403–406. https://doi.org/10.1016/0272-8842(95)94466-N.

[7] R.B. Figueira, C.J.R. Silva, E. V. Pereira, Organic–inorganic hybrid sol–gel coatings for metal corrosion protection: a review of recent progress, J. Coatings Technol. Res. 12 (2014) 1–35. https://doi.org/10.1007/s11998-014-9595-6.

[8] M.L. Zheludkevich, I.M. Salvado, M.G.S. Ferreira, Sol-gel coatings for corrosion protection of metals, J. Mater. Chem. 15 (2005) 5099–5111. https://doi.org/10.1039/b419153f.

[9] J.D. Mackenzie, Applications of the sol-gel process, J. Non. Cryst. Solids. 100 (1988) 162–168. https://doi.org/10.1016/0022-3093(88)90013-0.

[10] L.L. Hench, J.K. West, The Sol-Gel Process, Chem. Rev. 90 (1990) 33–72. https://doi.org/10.1021/cr00099a003.

[11] D. Wang, G.P. Bierwagen, Sol-gel coatings on metals for corrosion protection, Prog. Org. Coatings. 64 (2009) 327–338. https://doi.org/10.1016/j.porgcoat.2008.08.010.

[12] S. Zheng, J. Li, Inorganic-organic sol gel hybrid coatings for corrosion protection of metals, J. Sol-Gel Sci. Technol. 54 (2010) 174–187. https://doi.org/10.1007/s10971-010-2173-1.

[13] P. Innocenzi, M.O. Abdirashid, M. Guglielmi, Structure and properties of sol-gel coatings from methyltriethoxysilane and tetraethoxysilane, J. Sol-Gel Sci. Technol. 3 (1994) 47–55. https://doi.org/10.1007/BF00490148.

[14] J. Gallardo, A. Duran, I. Garcia, J.P. Celis, M.A. Arenas, A. Conde, Effect of sintering temperature on the corrosion and wear behavior of protective SiO2-based sol-gel coatings, J. Sol-Gel Sci. Technol. 27 (2003) 175–183. https://doi.org/10.1023/A:1023702701850.

[15] J.D. Mackenzie, E.P. Bescher, Physical Properties of Sol-Gel Coatings, J. Sol-Gel Sci. Technol. 19 (2000) 23–29. https://doi.org/10.1023/A.

[16] R. Ding, W. Li, X. Wang, T. Gui, B. Li, P. Han, H. Tian, A. Liu, X. Wang, X. Liu, X.

Gao, W. Wang, L. Song, A brief review of corrosion protective films and coatings based on graphene and graphene oxide, J. Alloys Compd. 764 (2018) 1039–1055. https://doi.org/10.1016/j.jallcom.2018.06.133.

[17] D. Prasai, J.C. Tuberquia, R.R. Harl, G.K. Jennings, K.I. Bolotin, Graphene: Corrosion-inhibiting coating, ACS Nano. 6 (2012) 1102–1108. https://doi.org/10.1021/nn203507y.

[18] A.J. López, A. Ureña, J. Rams, Wear resistant coatings: Silica sol-gel reinforced with carbon nanotubes, Thin Solid Films. 519 (2011) 7904–7910. https://doi.org/10.1016/j.tsf.2011.05.076.

[19] A.J. López, A. Rico, J. Rodríguez, J. Rams, Tough ceramic coatings: Carbon nanotube reinforced silica sol-gel, Appl. Surf. Sci. 256 (2010) 6375–6384. https://doi.org/10.1016/j.apsusc.2010.04.020.

[20] Y. Liu, H. Cao, Y. Yu, S. Chen, Corrosion protection of silane coatings modified by carbon nanotubes on stainless steel, Int. J. Electrochem. Sci. 10 (2015) 3497–3509.

[21] C.J. Brinker, G.C. Frye, A.J. Hurd, C.S. Ashley, Fundamentals of sol-gel dip coating, Thin Solid Films. 201 (1991) 97–108.

[22] D. Grosso, How to exploit the full potential of the dip-coating process to better control film formation, J. Mater. Chem. 21 (2011) 17033–17038. https://doi.org/10.1039/c1jm12837j.

[23] A.J. López, E. Otero, J. Rams, Sol-gel silica coatings on ZE41 magnesium alloy for corrosion protection, Surf. Coatings Technol. 205 (2010) 2375–2385. https://doi.org/10.1016/j.surfcoat.2010.09.027.

[24] J.R. Scully, Polarization resistance method for determination of instantaneous corrosion rates, Corrosion. 56 (2000) 199–217. https://doi.org/10.5006/1.3280536.

[25] G. Song, A. Atrens, D. StJohn, An Hydrogen Evolution Method for the Estimation of the Corrosion Rate of Magnesium Alloys, in: S.N. Mathaudhu, A.A. Luo, N. N.R., E.A. Nyberg, S. W.H. (Eds.), Essent. Readings Magnes. Technol., Springer, Cham, 2016: pp. 565–572. https://doi.org/https://doi.org/10.1007/978-3-319-48099-2_90.

[26] M. Stern, L. Geary, A Theoretical Analysis of the Shape of Polarization Curves, J. Electrochem. Soc. 104 (1957) 56–73. https://doi.org/10.1149/1.2428473.

[27] A. Atrens, W. Dietzel, The negative difference effect and unipositive Mg, Adv. Eng. Mater. 9 (2007) 292–297. https://doi.org/10.1002/adem.200600275.

[28] M. Zaharescu, L. Predoana, A. Barau, D. Raps, F. Gammel, N.C. Rosero-Navarro, Y. Castro, A. Durán, M. Aparicio, SiO2 based hybrid inorganic-organic films doped with TiO2-CeO2 nanoparticles for corrosion protection of AA2024 and Mg-AZ31B alloys, Corros. Sci. 51 (2009) 1998–2005. https://doi.org/10.1016/j.corsci.2009.05.022.

[29] P.C. Innocenzi, M. Guglielmi, M. Gobbin, P. Colombo, Coating of metals by the sol-gel dip-coating method, J. Eur. Ceram. Soc. 10 (1992) 431–436. https://doi.org/10.1016/0955-2219(92)90018-9.

Figure Captions

Fig. 1. SEM micrographs of the MWCNTs (a) and the COOH-GNPs (b) used as nano-reinforcement.

Fig.2. Four different coating configurations: SG monolayer, SG+SG multilayer, SG+SG/CNT multilayer, SG+SG/GNP multilayer.

Fig.3. Experimental set-up. (a) Three-electrode cell configuration for electrochemical polarization resistance tests. (b) Sample mounted for hydrogen evolution test.

Fig.4. (a) Cross-section view of a SG+SG/CNT multilayer coating. (b) Tilted view of a SG+SG/GNP multilayer coating configuration.

Fig.5. Nanocharge dispersions. (a) MWCNTs aggregate embedded in the sol-gel coating. (b) Detail of MWCNTs aggregate. (c) TEM micrograph of GNPs. (d) GNPs embedded in the sol-gel coating.

Fig.6. Average coating thickness for the four different coating systems.

Fig.7. Average linear polarization resistance (*Rp*) values for the different coating systems.

Fig.8. Corrosion products layer on uncoated samples after 24 hours (a) and 48 hours (b) of immersion in 3.5 wt% NaCl solution.

Fig.9. Evolution of the corrosion process over 72 hours of immersion in 3.5 wt% NaCl medium for all the coating configurations.

Fig.10. Anodic-cathodic polarization curves for 1 hour (a) and 24 hours (b) of immersion in 3.5 wt% NaCl.

Fig.11. H_2 evolution test for 168 h of immersion in 3.5 wt% NaCl and detail of the first 48 h of immersion.

Fig.12. Corrosion rate of the Mg alloy coated with the different coating systems after 168 h of immersion in 3.5 wt% NaCl.

Fig.13. Corrosion prints after 168 h of immersion of the different coating systems: (a) Uncoated, (b) SG, (c) SG+SG, (d) SG+SG/CNT, (e) SG+SG/GNP.

Fig.14. Cross-section micrographs of the progression of the corrosion process for all of the tested samples: (a) Uncoated, 1 hour of immersion. (b) Uncoated, 24 hours of immersion. (c) Uncoated, 48 hours of immersion. (d) SG, 1 hour of immersion. (e) SG, 24 hours of immersion. (f) SG, 48 hours of immersion. (g) SG+SG, 1 hour of immersion. (h) SG+SG, 24 hours of immersion. (i) SG+SG, 48 hours of immersion. (j) SG+SG/CNT, 1 hour of immersion. (k) SG+SG/CNT, 24 hours of immersion. (l) SG+SG/CNT, 48 hours of immersion. (m) SG+SG/GNP, 1 hour of immersion. (n) SG+SG/GNP, 24 hours of immersion. (o) SG+SG/GNP, 48 hours of immersion.

Fig.15. (a) Corrosion breaking point in a monolayer SG coating configuration. (b) Corrosion products spreading in the interface between the substrate and the SG monolayer coating.

Fig.16. (a) EDX in the zone marked as A in Fig 14. (b) EDX in the zone marked as B in Fig 14.

Fig.17. Coating degradation and substrate corrosion mechanism scheme.